Data-driven clay-fouled ballast permeability assessment using analytical-numerical and machine learning approaches

Koohmishi, Mehdi; Guo, Yunlong

DOI
10.1016/j.trgeo.2023.101151

Publication date
2023

Document Version
Final published version

Published in
Transportation Geotechnics

Citation (APA)
Koohmishi, M., & Guo, Y. (2023). Data-driven clay-fouled ballast permeability assessment using analytical-numerical and machine learning approaches. *Transportation Geotechnics*, *43*, Article 101151. https://doi.org/10.1016/j.trgeo.2023.101151

Transportation Geotechnics 43 (2023) 101151

Contents lists available at ScienceDirect

Transportation Geotechnics

journal homepage: www.elsevier.com/locate/trgeo

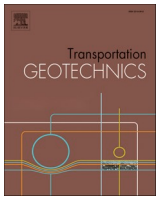

Data-driven clay-fouled ballast permeability assessment using analytical-numerical and machine learning approaches

Mehdi Koohmishi [a,*], Yunlong Guo [b,*]

[a] Department of Civil Engineering, Faculty of Engineering, University of Bojnord, Bojnord, Iran
[b] Faculty of Civil Engineering and Geosciences, Delft University of Technology, Delft 2628CN, Netherlands

ARTICLE INFO

Keywords:
Water height
Flume test
Clay-fouled ballast
Darcy's law
Machine learning
XGBoost
Steady-state flow

ABSTRACT

The occurrence of ballast contamination or fouling frequently results in a sudden decline in the capacity of railway ballasted tracks. Considering the various sources of ballast fouling, clay is the most severe one for causing a drastic reduction in the drainage capacity of the ballast layer. In the current study, we utilized a large-scale flume test to measure the water height along the cross-section of the clay-fouled ballast. Subsequently, an analytical–numerical (A-N) approach was developed to simulate the movement of water through porous media under steady-state conditions, while also considering the flow regime. This A-N approach was validated using the results of flume tests. Finally, the validated A-N approach was employed to generate a dataset and develop machine learning models for predicting water height. The characterized machine learning models included random forest regression (RFR), support vector machine (SVM), and extreme gradient boosting (XGBoost). Various variables, such as ballast gradation, fouling ratio, bed slope, rainfall rate, and water height on the side ditch, were incorporated into the machine learning models to reveal the contribution of each individual variable. Results show that for clean ballast, the incorporation of a nonlinear model between flow velocity and hydraulic gradient in the A-N approach is crucial to properly estimate the experimental measurements. However, a comparison of the water height measured via the flume test and the water level estimated based on the A-N approach confirms the suitability of the linear model, i.e., Darcy's law, for the water flow regime through clay-fouled ballast. According to the machine learning results, particularly those from the XGBoost model, which was characterized as the elite model, the rainfall rate and the fouling index emerged as the most influential variables affecting the water height in the clay-fouled ballast layer of the railway track.

Introduction

Railway ballasted tracks are the most commonly used structure worldwide [26]. Among the major components of the track structure, the ballast layer is the most crucial part of the substructure, specially functioning as a drainage layer [18]. This granular medium facilitates the process of adjusting the geometry of the track. However, fouling among ballast particles is a major deterioration factor that affects the proper performance of the course (Hai [16,33,44]. In relation to various factors, the infiltration of clay—from either underlying layers or the surface—into the ballast layer is identified as a source causing acceleration of track failure [20,43].

In this context, Huang et al. [17] highlighted the reduction in strength properties of ballast contaminated with clay and mineral filler. Without the interference of water, coal dust was identified as the most detrimental fouling agent. Furthermore, Danesh et al. [8] observed a more severe impact of clay fouling on shear strength compared to sand contamination by conducting a direct shear test. As noted by Indraratna et al. [19], soils with low-to-medium plasticity were more prone to mud pumping. Given the various issues associated with clay fouling in the ballast layer, inadequate hydraulic conductivity and water ponding are key factors that negatively influence the drainage competence of both this layer and the overall track structure.

The measurement of hydraulic conductivity is a well-established approach to determining the drainage capacity of ballast materials [15]. For instance, the interrelation between fouling, permeability, and resistivity demonstrated that using clay as a fouling material, compared to fines produced by ballast degradation, led to a more significant reduction in permeability [32,34,22]. Moreover, hydraulic conductivity measurements of ballast fouled with distinct fine particles, including

* Corresponding authors.
E-mail addresses: m.koohmishi@ub.ac.ir (M. Koohmishi), yunlong.guo@tudelft.nl (Y. Guo).

https://doi.org/10.1016/j.trgeo.2023.101151
Received 2 August 2023; Received in revised form 20 October 2023; Accepted 5 November 2023
Available online 8 November 2023

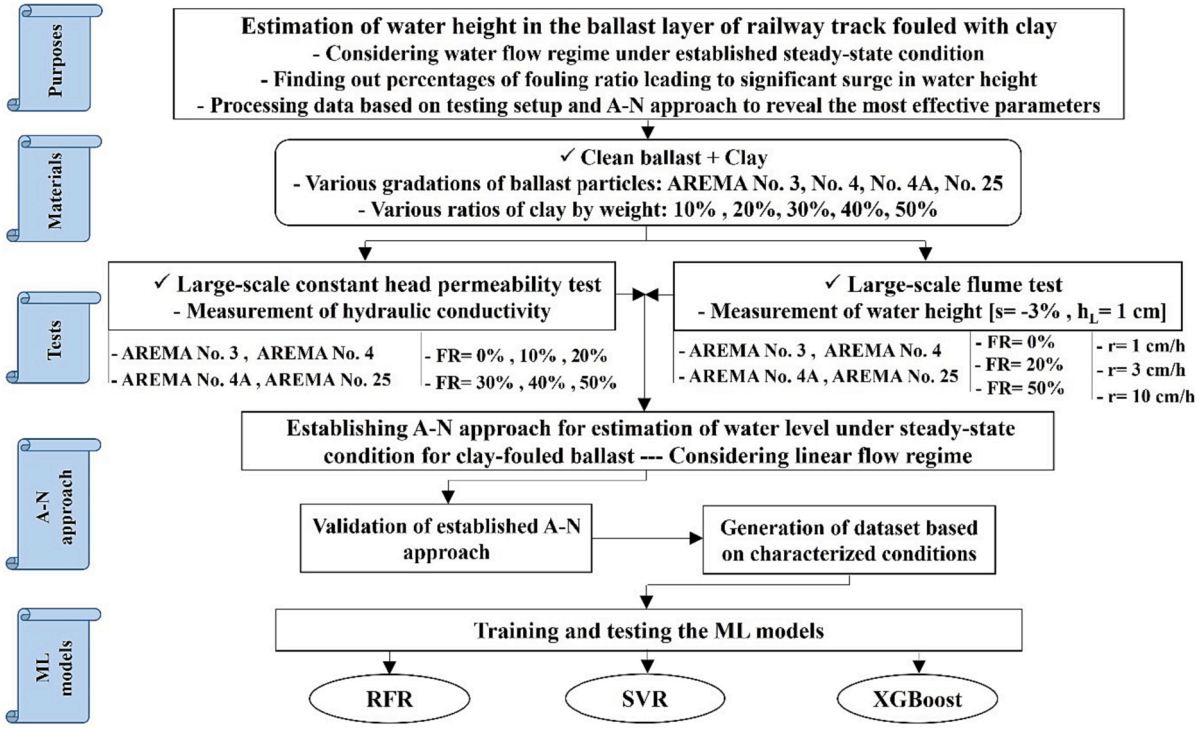

Fig. 1. Outlined description of the present study for estimation of water height in the clay-fouled ballast layer under steady-state flow condition.

kaolin, limestone, and crushed ballast were performed in [9], which revealed the most drastic effect was kaolin. Koohmishi [24] conducted the constant-head permeability test on degraded ballast particles fouled with clay. The experimental observations corroborated that the hydraulic conductivity of degraded ballast was still acceptable, however, the intrusion of clay led to an unacceptable drainage capacity of ballast layer. Recently, Mayuranga and Navaratnarajah [29] carried out a full-scale permeability test on ballast fouled with sandy lean clay. The results showed that the reduction in hydraulic conductivity exceeded 90 % when the void contamination index (VCI) was above 25 %.

An effective and efficient means for assessing railway track drainage is estimating the water height along the cross-section of the substructure. In this regard, Heyns [13] conducted laboratory flume tests to investigate subballast drainage, considering different variables such as rainfall intensity, subballast thickness, and slope of the subballast/subgrade interface. The use of a mixture of coarse sand and gravel as a clean subballast material was proposed to reduce the likelihood of subballast saturation. Tennakoon et al. [37] proposed ballast cleaning using undercutting when the top ballast had VCI greater than 50 % representing poor drainage capacity.

Machine learning approaches for estimating and predicting physical properties, such as the permeability coefficient were feasible in earlier

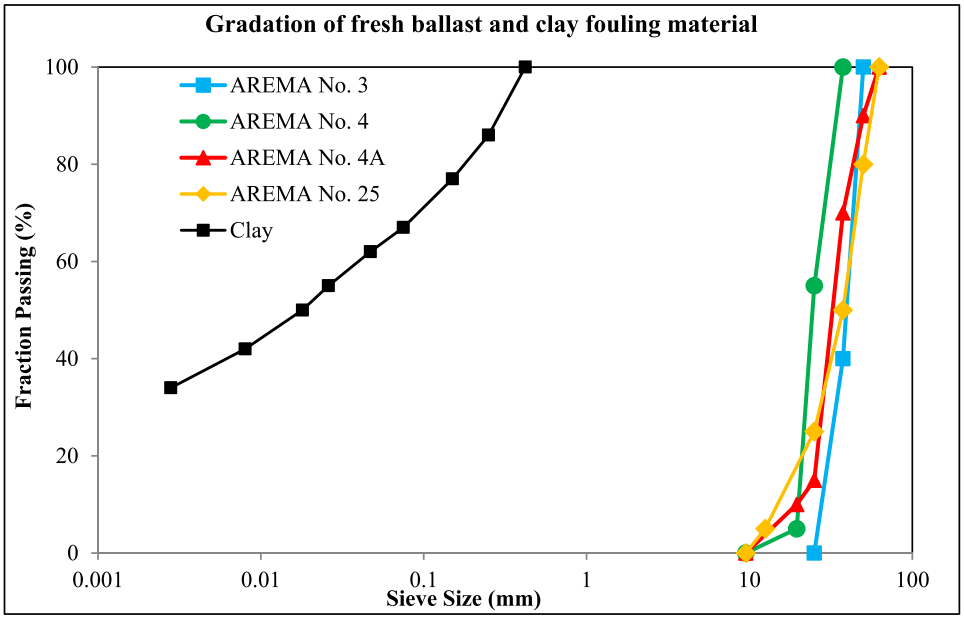

Fig. 2. Gradation curves of fresh crushed ballast particles and kaolin representing the clay fouling material.

Table 1
Main properties relevant to characterized gradation curves for ballast particles.

Grading type	d_{max} (mm)	d_{min} (mm)	d_{10} (mm)	d_{60} (mm)	C_u
AREMA No. 3	50.0	25.0	28.1	41.2	1.47
AREMA No. 4	37.5	9.5	20.1	26.4	1.31
AREMA No. 4A	62.5	9.5	19.5	35.2	1.81
AREMA No. 25	62.5	4.75	15.0	41.3	2.75

studies. For example, Araya and Ghezzehei [2] applied machine learning to a large database to predict the saturated hydraulic conductivity of soil, identifying the 10th percentile particle diameter as an important predictor. Menke et al. [30] employed the extra-trees regression to bridge between the pore scale and Darcy scale for the permeability of microporous carbonate. Moreover, Tian et al. [38] used a combination of artificial neural network and genetic algorithm to predict permeability by generating different porous media. The results confirmed that tortuosity and the number of pores were characterized as the effective parameters inversely proportional to permeability. Furthermore, Azarhoosh and Koohmishi [4] noted that the random forest (RF) model was superior in predicting the hydraulic conductivity of granular specimens composed of large-sized aggregates.

The aforementioned studies have thoroughly investigated the permeability of clay-fouled ballast [24,32,37]. However, determining water height in porous media, instead of measuring hydraulic conductivity, can provide a more practical appraisal of drainage capacity. Indeed, identifying which fouling ratios and rainfall rates lead to a significant surge in water height would be helpful for implementing maintenance activities at appropriate times. This is particularly true when considering that the extent of contamination, whether determined based on destructive or non-destructive tools, could influence these timings. In this regard, no study has been conducted to determine the water height along the cross-section of a ballast layer contaminated with clay material. Additionally, conducting large-scale experimental programs, such as flume tests, to assess the drainage performance of a ballast layer can be time-consuming. Therefore, establishing compound approaches like analytical–numerical (A-N) methods, alongside experimental setups, is a viable solution to this problem. Furthermore, the porosity of fresh ballast aggregate dictates the turbulence of the flow regime, but additional fouling would inevitably lead to a transition in the flow regime. This transition in the flow regime condition can also be incorporated into these approaches.

In this study, we establish a composite procedure to obtain the water level in the clay-fouled ballast layer, using a large-scale flume test and the characterized analytical–numerical (A-N) approach. This A-N approach takes into account different variables, such as aggregate gradation, fouling level, ballast bed slope, rainfall rate, and water height on the side ditch; while also considering laminar, transitional, or turbulent flow regimes under steady-state conditions. This approach is used to generate a dataset in which these variables are considered. Subsequently, machine learning (ML) models—including random forest regression (RFR), support vector regression (SVR), and extreme gradient boosting (XGBoost)—are trained and tested based on the prepared dataset. Finally, the best-performing ML model is used to delineate the importance of distinct characterized variables. Fig. 1 succinctly illustrates the outline of the present study.

Materials and laboratory test setup

Materials

– Fresh crushed ballast

The sieve-size divisions of the crushed ballast particles, derived from a basalt parent rock, comply with the gradation bands defined by AREMA [3]. These are designated as AREMA No. 3, No. 4, No. 24, and No. 25, as illustrated in Fig. 2. The ballast has a specific gravity of 2.72 and a water absorption rate of 0.56 %. Table 1 presents the main properties associated with these characterized gradation curves.

– Clay soil, simulation of ballast fouling

In the current study, kaolin was selected as the external fouling material. This fine-grained soil has a considerable plasticity index, with a liquid limit of 53 % and a plastic limit of 29 %. Fig. 2 also shows the gradation curve of this clay soil.

Test setup

Large-scale constant-head permeability test

Fig. 3 schematically illustrates the large-scale permeability testing apparatus. This apparatus consists of a large reservoir used to control the water head applied to the specimen and a cylindrical, smaller repository designed for placing the granular specimen. For each defined hydraulic head difference, the water collected after moving through the granular media is weighed to determine the flow velocity in relation to the applied hydraulic gradient. Further details have been provided in a preceding study conducted by [25].

Large-scale flume test

The large-scale flume testing apparatus primarily consists of a reservoir, with a length of 2.0 m, a width of 0.6 m, and also a height of

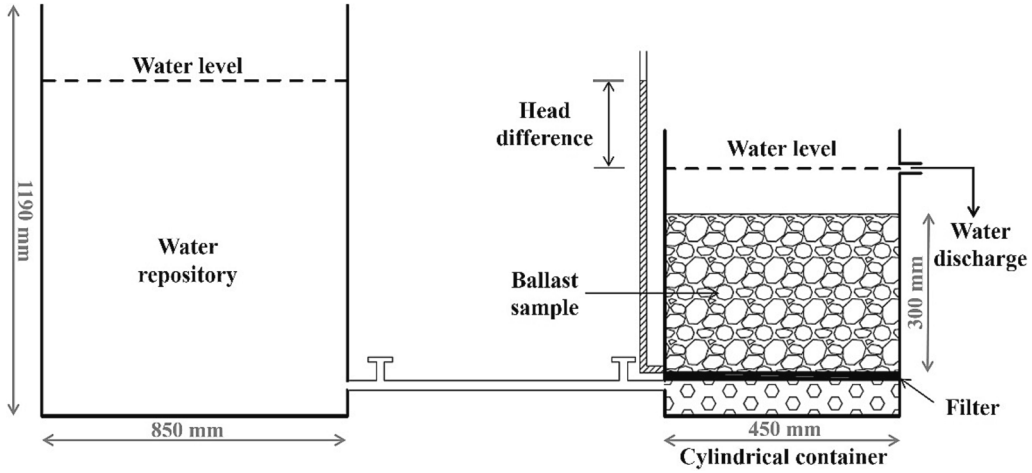

Fig. 3. Schematic drawing of constant-head permeability tester [25].

a Reservoir and rainfall generation system

b Nozzle-type rainfall simulator

c Piezometers installed for controlling the water level

c Clean ballast particles in the reservoir: AREMA No. 4

d Clean ballast particles in the reservoir: AREMA No. 4A

Fig. 4. Details of large-scale flume test.

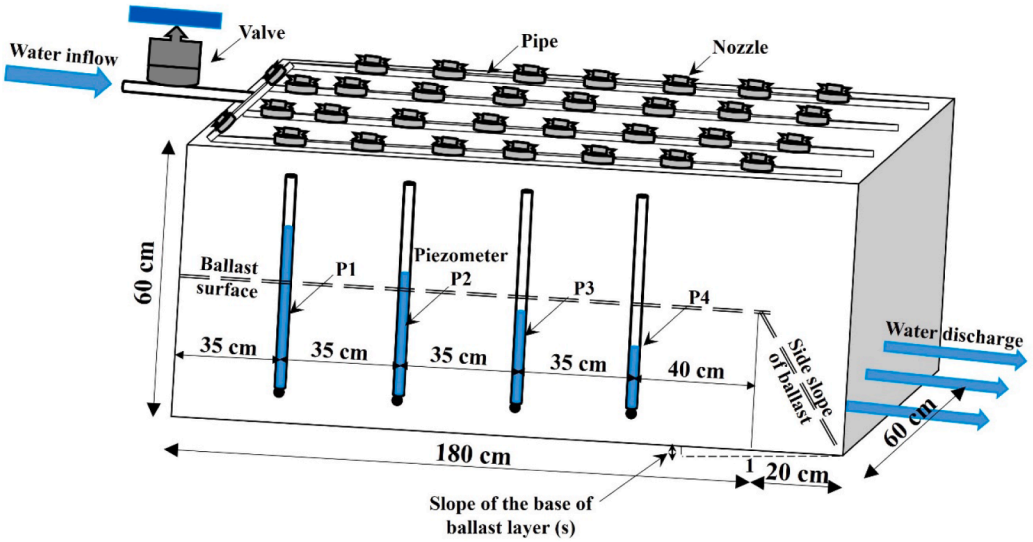

e Schematic illustration of the large-scale flume apparatus

Fig. 4. (*continued*).

0.6 m. Ballast samples, with a thickness of 0.3 m and whether clean or fouled with clay, are densely placed in this repository. A rain generation system is employed to distribute simulated continuous rainfall over the prepared specimen. The characterized prototype mirrors the half-sized cross-section of a ballast layer, from the track centreline towards the side ditch. It also simulates water movement through this granular media. This goal is achieved by keeping the upper side closed and the lower side open, while also maintaining a specific bed slope. To control the water height throughout the cross-section of this porous course, four piezometers are installed within the ballast bed. Fig. 4 illustrates the details of the flume test manufactured for water height measurement.

Quantification of ballast fouling

Distinct proportions of clayey soil (kaolin) by dry weight of ballast were added to account for various fouling ratios (FR), which represent the dry mass of clay divided by the dry mass of the ballast. The values of FR used in this study were 10 %, 20 %, 30 %, 40 %, and 50 %. As noted by Parsons et al. [32], the fouling index, introduced by Selig and Waters [35], represents the sum of the percentages of particles by weight passing through both sieve No. 4 and sieve No. 200. This is considered a superior index, especially when evaluating ballast hydraulic conductivity. Given the gradation curves for both ballast particles and kaolin, the aforementioned FR values correspond to 15 %, 28 %, 39 %, 48 %, and 56 % of the fouling index. To simulate the deposition of fine particles onto the track, kaolin was initially spread over the intermittent layers of compacted ballast specimens, followed by blowing the tamping rod. Fig. 5 illustrates ballast particles contaminated with various ratios of clay.

Analytical-numerical approach established for modelling water flow through ballast layer

Characterizing the water flow regime

The primary measurements from the constant-head permeability test involve determining the variations in water flow velocity through the granular specimen with respect to the applied hydraulic head. To this end, Table 2 presents the established relationships that elucidate the connection between flow velocity (V) and hydraulic gradient (i), encompassing both linear and non-linear trend lines.

In Table 2, characterizing ballast as porous granular media, the establishment of a nonlinear formula, such as Izbash's law, can appropriately account for the relationship between V and i. The further infiltration of clay particles diminishes the turbulence of water flow through this media, thus making a linear formula, specifically Darcy's law, more appropriate.

A-N approach for estimation of water surface

The schematic cross-section of the ballast layer, as illustrated in Fig. 6, characterizes the ballast bed as an impermeable surface, which leads to a transverse water flow through the ballast layer. Therefore, considering the unit length of this layer, the transverse flow equates to the rainfall rate over the considered surface. This characterized condition results in the following formula:

$$V = \frac{rx}{h(x)} \tag{1}$$

V = Water flow velocity (cm/s)
x = Distance from the centreline of the railway track (cm)
h(x) = Elevation of water in the ballast layer (cm)
r = Constant rainfall rate (cm/s)

Incorporation of preceding equation for flow velocity in Izbash's law, results in:

$$\frac{dH}{dx} = -c_1\left(\frac{rx}{h}\right)^n \tag{2}$$

Given the transverse slope of the ballast layer from the centreline towards the side ditches, the hydraulic gradient is composed of a gradient from the ballast bed slope and a gradient from the saturated thickness of the ballast layer, as expressed below:

$$\frac{dH}{dx} = \frac{dh}{dx} + s \tag{3}$$

s = Slope of the bed of ballast layer (%)

Combining Eqs. (2) and (3) leads to the main differential equation for steady-state flow through the porous layer given by:

a.1

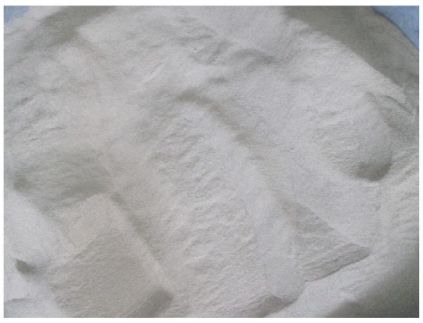

a.2

a Kaolin used as fouling material

b.1 FR: 20%

c.1 FR: 20%

b.2 FR: 30%

b.3 FR: 50%

c.2 FR: 50%

b Clay-fouled ballast in the main reservoir of permeability testing apparatus

c Clay-fouled ballast in the reservoir of flume testing apparatus

Fig. 5. Clay-fouled ballast in the main reservoirs of permeability and flume testing apparatus considering various fouling ratios.

Table 2
Formulae established for characterizing the relationship between water flow velocity and applied hydraulic gradient considering flow regime.

Author (Year)	Formula	Description
Darcy [10]	$V = k\left(\frac{\Delta H}{L}\right) = ki$	Linear trend line
Fwa et al. [11]	$V = k_1 i^m$	Nonlinear trend line - Power law
Izbash [21]	$i = \frac{dH}{dl} = -c_1 V^n$	Nonlinear trend line - Power law

V: Water flow velocity (cm/s); L: Distance in the direction of water flow (cm); H: Hydraulic head (cm); ΔH: Hydraulic head difference between two points (cm);
i: Applied hydraulic gradient;
k: Hydraulic conductivity (cm/s); k_1, m, c_1, n: Experimental coefficients.

$$\frac{dh}{dx} = -c_1\left(\frac{rx}{h}\right)^n - s \tag{4}$$

To further separate the Eq. (4), the following new variable is defined:

$$\eta = \frac{h}{x} \tag{5}$$

Differentiating the new defined variable with respect to x:

$$\frac{dh}{dx} = \eta + x\frac{d\eta}{dx} \tag{6}$$

Substitution of the Eq. (6) and new defined variable η into the differential equation (4), results in:

$$-x\frac{d\eta}{dx} = c_1\left(\frac{r}{\eta}\right)^n + \eta + s \tag{7}$$

Establishing further arrangement, the Eq. (8) is derived:

$$-\frac{dx}{x} = \frac{\eta^n d\eta}{\eta^{n+1} + s\eta^n + c_1 r^n} \tag{8}$$

Considering Fig. 6, the boundary condition of x = L, while h(x) = h_L is incorporated to solve this differential equation by establishment of fourth order Runge-Kutta method. The characterized boundary condition represents the water height on ditch located at right-hand side of the ballast layer.

Details of process of training and testing the ML models

Input/output dataset and evaluation method

As shown in Fig. 7.a, the dataset, validated based on the A-N approach estimations, consists of 1200 input–output data points. The inputs are aggregate gradation (C_u), fouling ratio (FR), bed slope (s), rainfall rate (r), and boundary condition (h_L), and the outputs are average water height (h_{Ave}) and maximum water height (h_{Max}). Based on previous studies [4,23], 70 % of the entire dataset was used to train the ML models, and the remaining 30 % was used as the testing dataset. The functions are defined as follows:

$$h_{Ave} = f(C_u\ ,\ FR\ ,\ s\ ,\ r\ ,\ h_L) \tag{9}$$

$$h_{Max} = f(C_u\ ,\ FR\ ,\ s\ ,\ r\ ,\ h_L) \tag{10}$$

The robustness of ML models established for prediction of water height in the ballast layer is evaluated by computing the following indices [14,27,31]:

$$R^2 = \left[\frac{\sum_{i=1}^{n}(y-\mu_y)(\hat{y}_i-\hat{\mu}_y)}{\sqrt{\sum_{i=1}^{n}(y_i-\mu_y)^2\sum_{i=1}^{n}(\hat{y}_i-\hat{\mu}_y)^2}}\right]^2 \tag{11}$$

$$RMSE = \sqrt{\sum_{i=1}^{n}(y_i-\hat{y}_i)\Big/n} \tag{12}$$

$$VAF = \left(1-\frac{Var|y-\hat{y}|}{Var(y)}\right)\times 100 \tag{13}$$

R^2 = Coefficient of determination
RMSE = Root mean square error
VAF = Variance account for
y = Actual values of $y_1, y_2, \cdots, y_n$
$\hat{y}$ = Predicted values of $\hat{y}_1, \hat{y}_2, \cdots, \hat{y}_n$
$\mu_y = E(y)$ = Average value of y
$\hat{\mu}_y = E(\hat{y})$ = Average value of $\hat{y}$

Cross-validation and grid search implementation

A 5-fold cross-validation procedure was used, which is a resampling method where the dataset is divided into five portions. Four subsets are

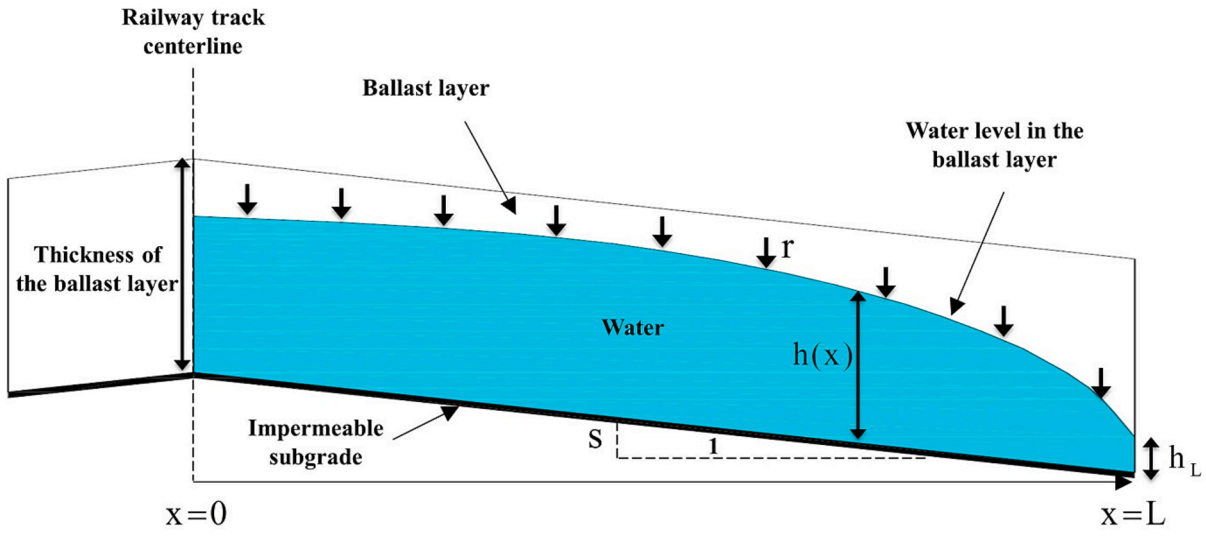

Fig. 6. Schematic cross-section of the ballast layer of the railway track substructure (after [6].

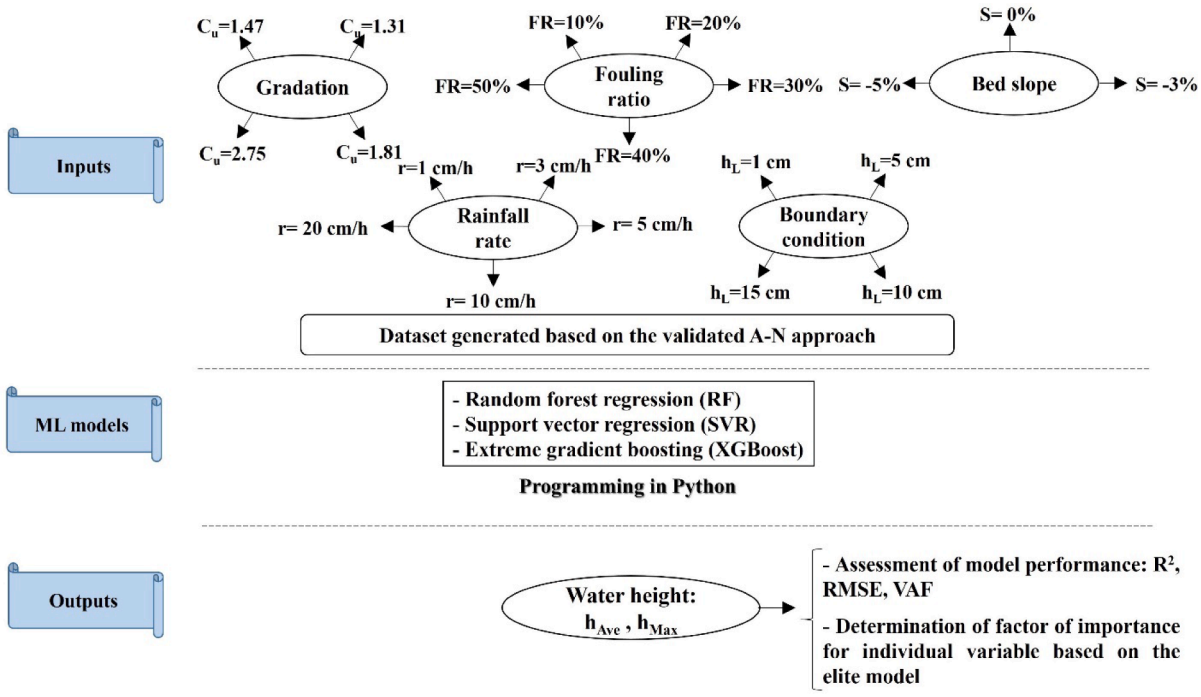

a Input/output dataset of established ML models and evaluation method

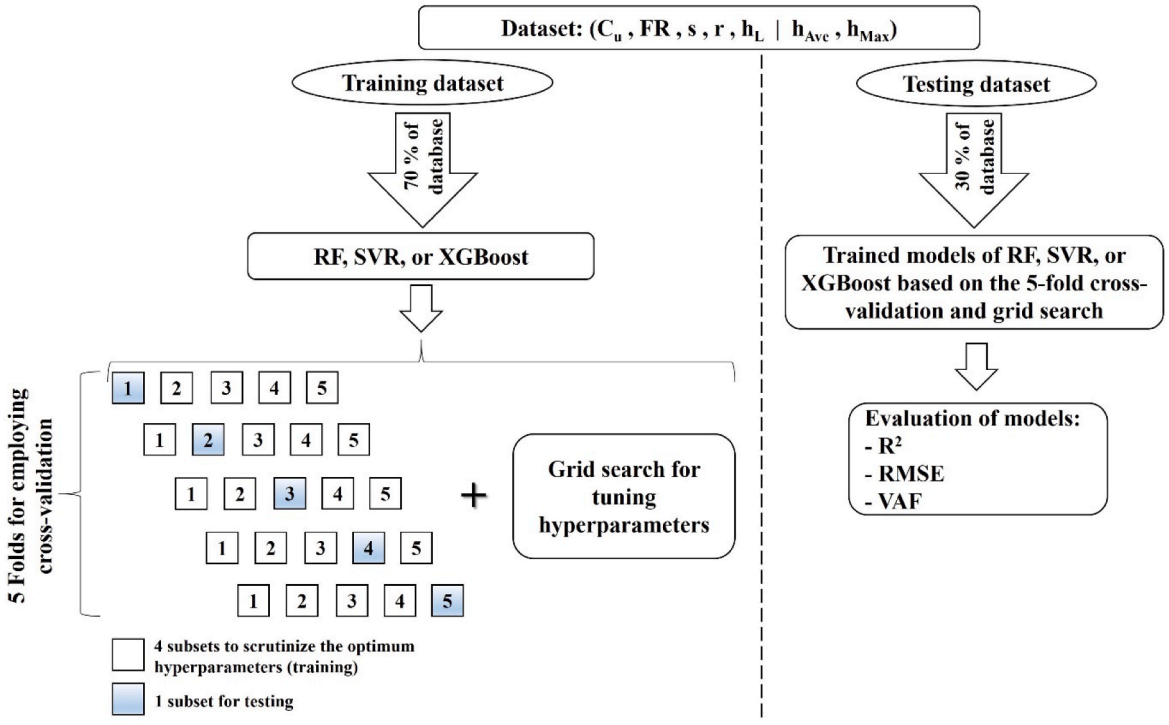

b Process of data split by establishment of cross-validation

Fig. 7. Details of process of training and testing the ML models.

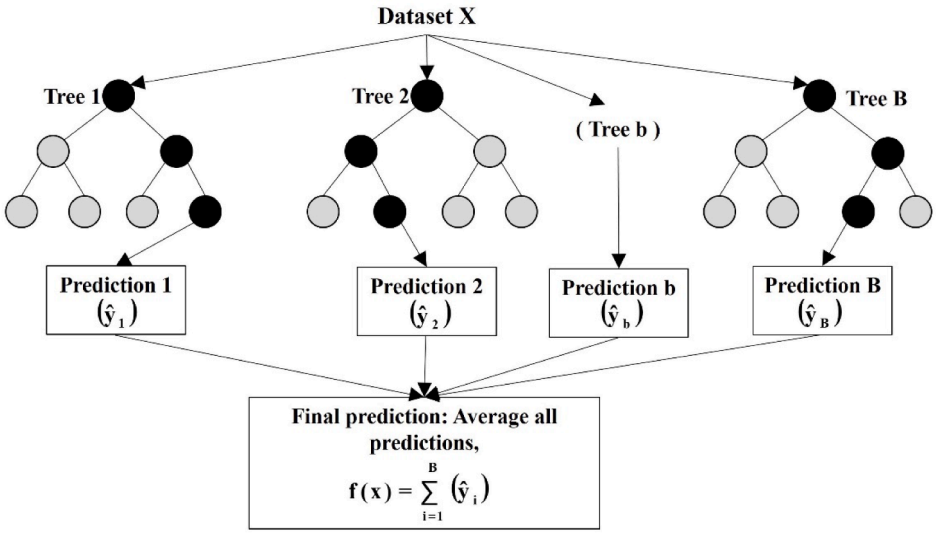

c.1 RFR

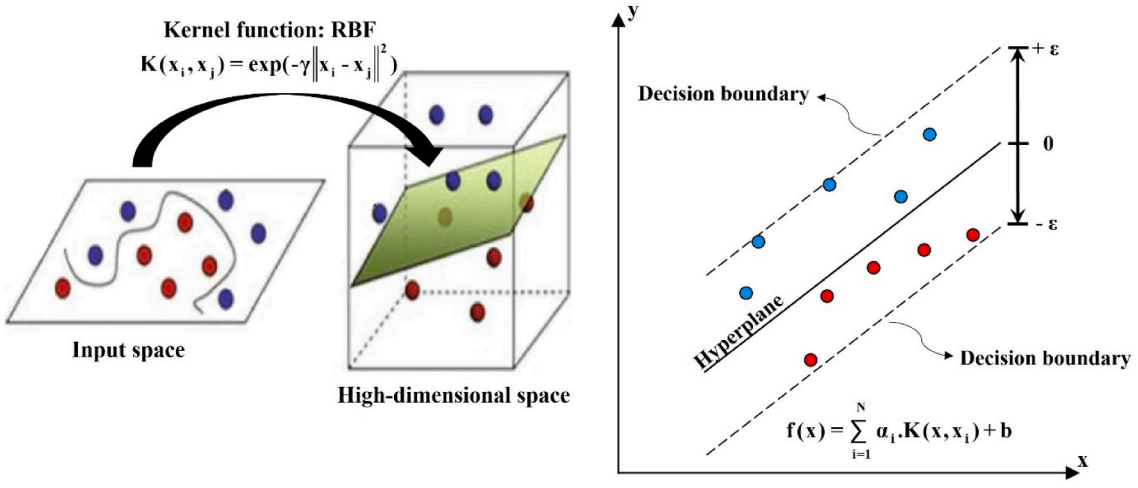

c.2 SVR

Fig. 7. (*continued*).

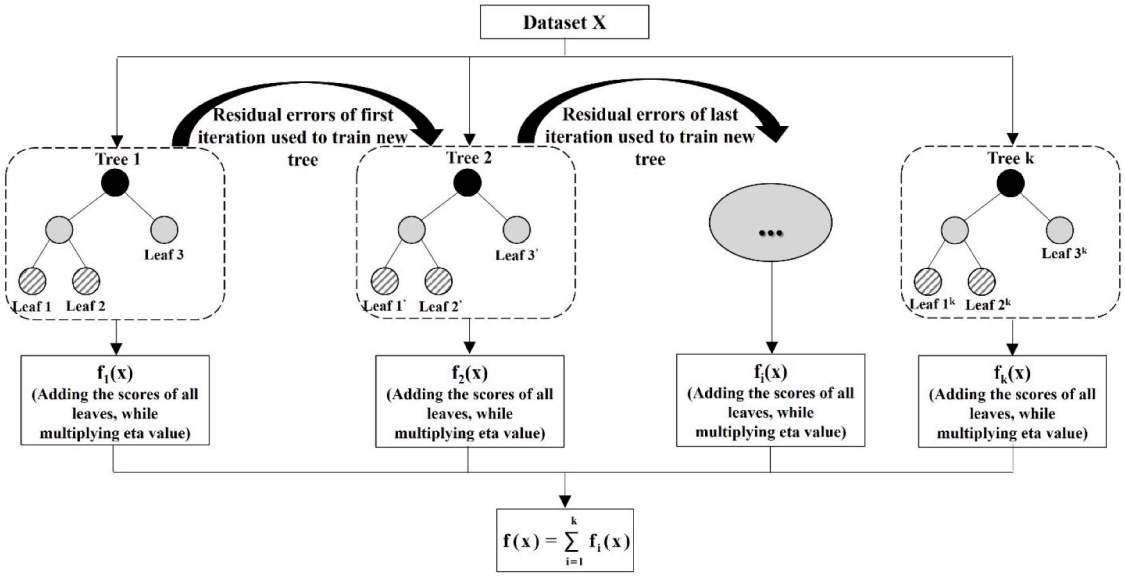

c.3 XGBoost

c Graphical representation of established ML models

Fig. 7. (*continued*).

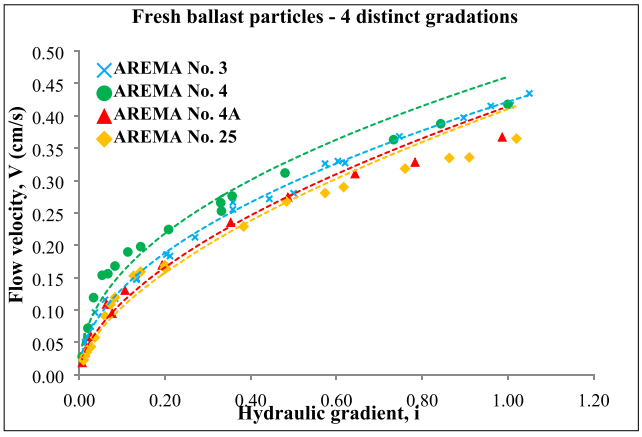

a Clean ballast

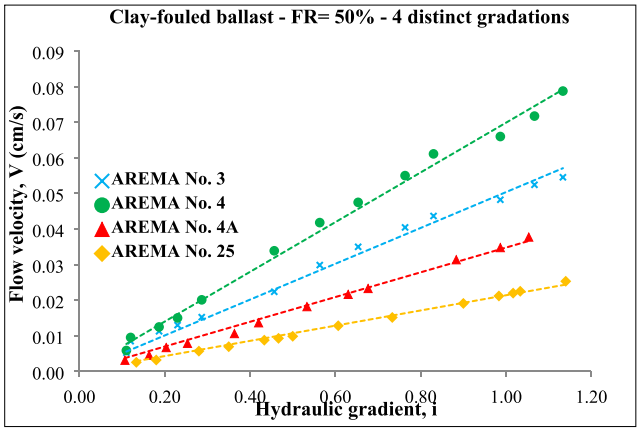

b Clay-fouled ballast: Highly-fouled (50% of FR)

Fig. 8. Variation of flow velocity with applied hydraulic gradient.

used as training data, and the remaining subset is used as testing data [39]. In the current study, as illustrated in Fig. 7.b, this process is repeated on the 5 folds of the training dataset, and then the average of the models is applied to the remaining 30 % of all data, designated as the testing data. Furthermore, the grid search method is concurrently utilized to tune hyperparameters and find the optimal model. In this regard, all possible values are tested to reveal the best hyperparameters that form the structure of the model.

ML models

Random forest regression

Introduced by Breiman [5], the Random Forest Regression (RFR) approach is based on building multiple decision trees on categorized samples, with the final output predicted based on the average values derived from these trees. The ability to handle continuous variables makes this supervised ML method applicable for regression prediction. The initial stage of selecting subsets from the entire dataset is known as bagging, while the final step of generating output based on the results of the decision trees is defined as aggregation. Some of the key hyperparameters relevant to the structure of RFR include: the number of trees (n_estimators); the maximum number of levels in an individual regression tree (max_depth); and the minimum number of data points allowed in a leaf node (min_samples_leaf).

Support vector machine

The Support Vector Regression (SVR) approach seeks to find a function, or hyperplane, that approximates the relationship between input and output in a continuous space, while also minimizing the prediction error (as illustrated in Fig. 7.c). As proposed by Vapnik [40], the kernel function incorporated in this ML method enables the consideration of non-linear relationships. It transforms the input data into a higher-dimensional space to effectively model the relationship with a linear decision boundary. Using the radial basis function (RBF) as a kernel function, two specific hyperparameters are considered: the regularization parameter (C), and the width of the kernel function (Gamma). The value of the regularization parameter controls the

Table 3
Summary results of large-scale constant-head permeability test.

Gradation	**a** Clean ballast specimens						Linear model	
	Nonlinear models							
	c_1	n	R^2	k_1 (cm/s)	m	R^2	k (cm/s)	R^2
AREMA No. 3	5.378	1.972	0.988	0.422	0.501	0.988	0.493	0.733
AREMA No. 4	4.236	2.019	0.936	0.460	0.464	0.936	0.537	0.2
AREMA No. 4A	4.448	1.733	0.985	0.415	0.568	0.985	0.454	0.755
AREMA No. 25	4.183	1.653	0.981	0.410	0.594	0.981	0.435	0.736

FR (%)	**b** Clay-fouled ballast specimens			
	k (cm/s) - Establishing Darcy's law Gradation of ballast particles			
	AREMA No. 3	AREMA No. 4	AREMA No. 4A	AREMA No. 25
10	0.480	0.530	0.442	0.390
20	0.395	0.455	0.360	0.320
30	0.235	0.265	0.200	0.165
40	0.115	0.145	0.085	0.057
50	0.050	0.070	0.035	0.021

complexity or simplicity of the function: a large C may lead to over-fitting, while a small C can result in under-fitting. A larger gamma value defines a more complex decision boundary that captures the details of the training data, while a smaller gamma creates a smoother boundary.

Extreme gradient boosting

The XGBoost algorithm, developed by Chen and Guestrin [7], is a robust ensemble ML approach in which regression trees form the framework. As illustrated in Fig. 7.c, the algorithm minimizes the loss gradient while fitting the model, thereby correcting the prediction errors made by previous models. The major hyperparameters of this ML model include the number of trees (n_estimators), tree depth (max_depth), and learning rate (eta). Here, n_estimators defines the number of trees to be fitted. Max_depth determines whether a tree is shallow or deep; increasing max_depth represents further complexity in the model, raising the possibility of over-fitting. The eta value indicates the shrinkage weight applied to the scores of all leaves in every iteration, helping to prevent over-fitting and providing sufficient space for subsequent trees.

Results and discussion

Experimental results

Summary results of constant-head permeability test

The variations of water flow velocity with the hydraulic gradient are depicted in Fig. 8, and the coefficients of regressions applied to the experimental data, which represent the relationship between V and i, are summarized in Table 3. As illustrated, Darcy's law, a linear relationship, effectively characterizes the variation of flow velocity with the applied hydraulic gradient in the case of clay-fouled ballast. However, utilizing the nonlinear model, power law, is necessary for a more accurate representation of this trend in the case of clean ballast. The general trend increasingly conforms to a linear trendline as the fouling ratio rises. For instance, the exponent n of Izbash's law is around 2 for clean ballast particles of AREMA No. 3, while this coefficient approaches 1 under highly-fouled conditions. Similarly, for ballast particles with an initial gradation of AREMA No. 25, the value of k for highly-fouled ballast particles is roughly one twenty-fifth of that for clean aggregates.

Summary results of flume test

In this study, we conducted 36 flume tests with varying ballast gradations, fouling levels, and rainfall rates. Fig. 9 shows the measurements of water height in the 4 installed piezometers, taking into account the initial gradation of ballast particles, the fouling ratio, and the rainfall rate. As expected, the water height increases proportionally with the fouling ratio and rainfall rate. While the effect of aggregate gradation on water height is minimal in the case of clean ballast particles, it becomes significant when clay fouling occurs. Specifically, ballast with a more uniform gradation effectively stores water among the granular particles due to an increase in voids, even under fouled conditions. However, gradations with higher C_u values lead to a reduction of air voids between granular particles, a variation that becomes more pronounced in highly fouled conditions. Therefore, the gradation of granular particles not only affects the shear strength behaviour of ballast [41], but also this physical property influences the drainage potential of this porous layer.

Results of A-N approach

Validation of A-N approach

The observations derived from our laboratory experiments confirm that the water flow regime transitions from a turbulent to a laminar condition. To further evaluate the A-N approach's efficacy, the water surface estimations were compared based on the A-N model with measurements from the flume test, considering both linear and nonlinear models.

To solve the differential equation in Eq. (8), we set the 's' value at −3% and the length of the half-sized cross-section at 180 cm. These values were chosen to represent the typical dimensions of the ballast layer in railway track structures and to simulate the dimensions of the large-sized flume test. It was considered rainfall rates (r) of 1, 3, and 10 cm/h, as well as a boundary condition (h_L) of 1 cm, reflecting the values used in the flume test.

Considering the V-i curves derived from the permeability test for both clean and clay-fouled ballast specimens, we assumed values of 2 and 1.7 for the exponent 'n' in Izbash's law.

Considering n = 1, representing the linear flow condition, Eq. (8) is simplified as follows:

$$\frac{dx}{x} = \frac{\eta.d\eta}{-c_1 r - s\eta - \eta^2} \tag{14}$$

Considering n = 1.7, characterizing flow condition between laminar and turbulent:

$$\frac{dx}{x} = \frac{\eta^{1.7}.d\eta}{-c_1 r^{1.7} - s\eta^{1.7} - \eta^{2.7}} \tag{15}$$

Hence, defining $\eta = \varsigma^{10}$:

$$\frac{dx}{x} = \frac{\eta^{26}.d\eta}{-c_1 r^{1.7} - s\eta^{17} - \eta^{27}} \tag{16}$$

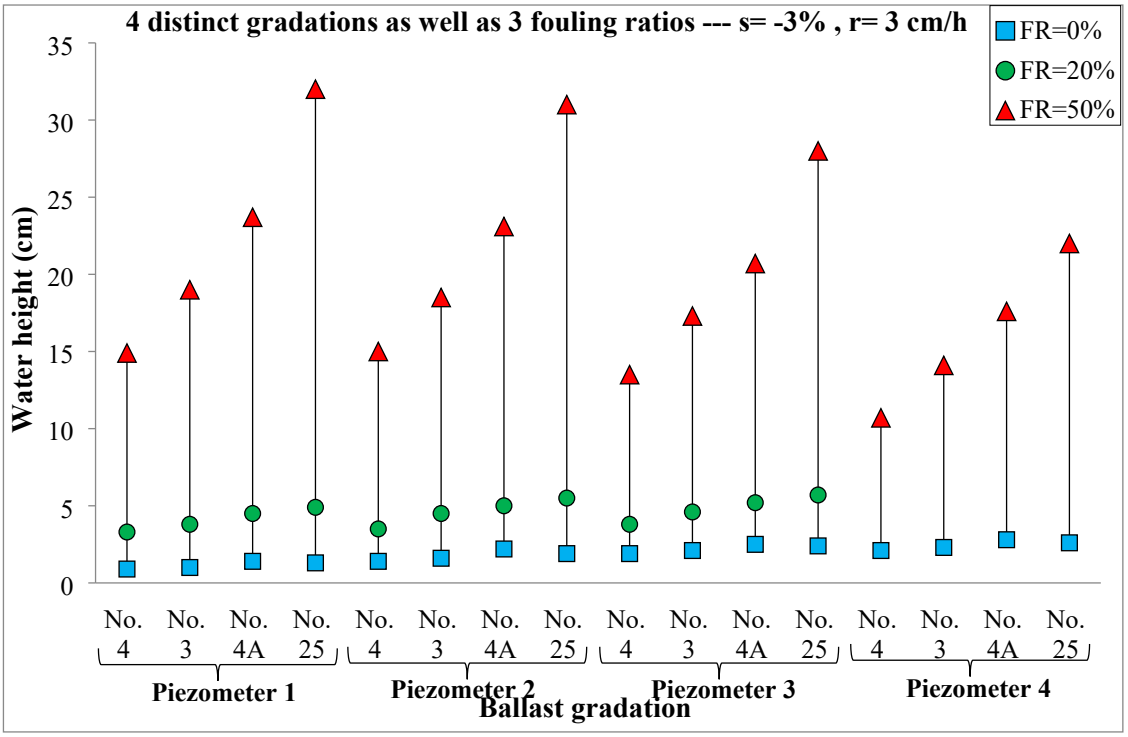

b r= 3 cm/h

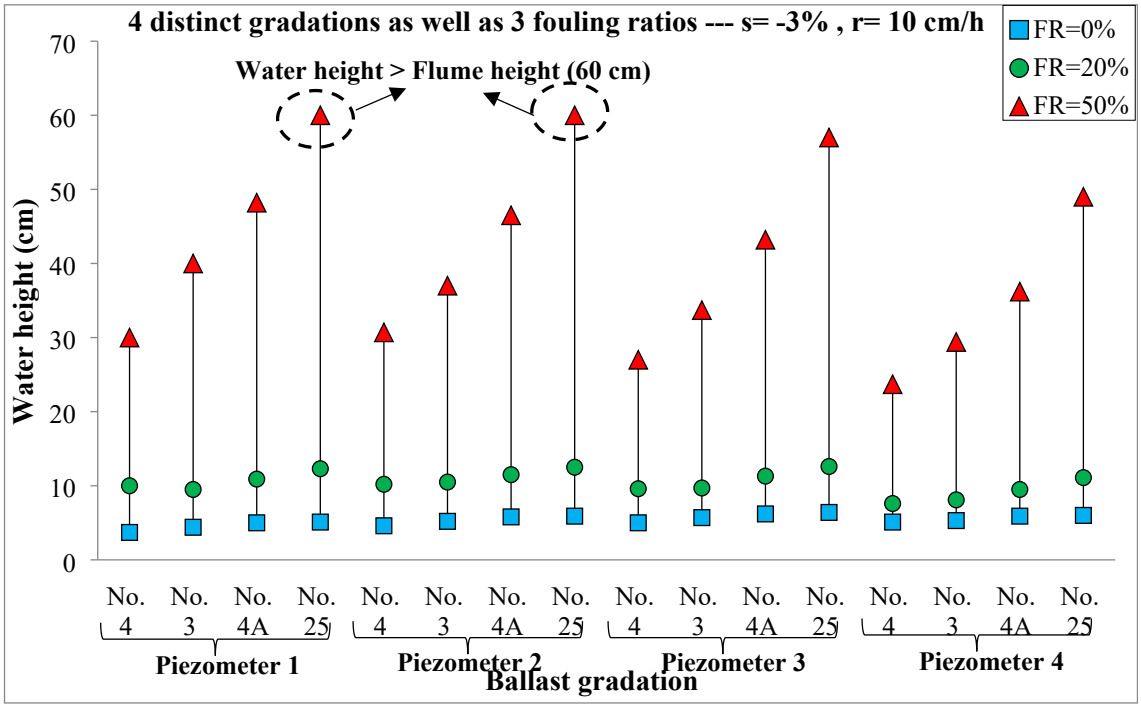

c r= 10 cm/h

Fig. 9. Summary results of large-scale flume test.

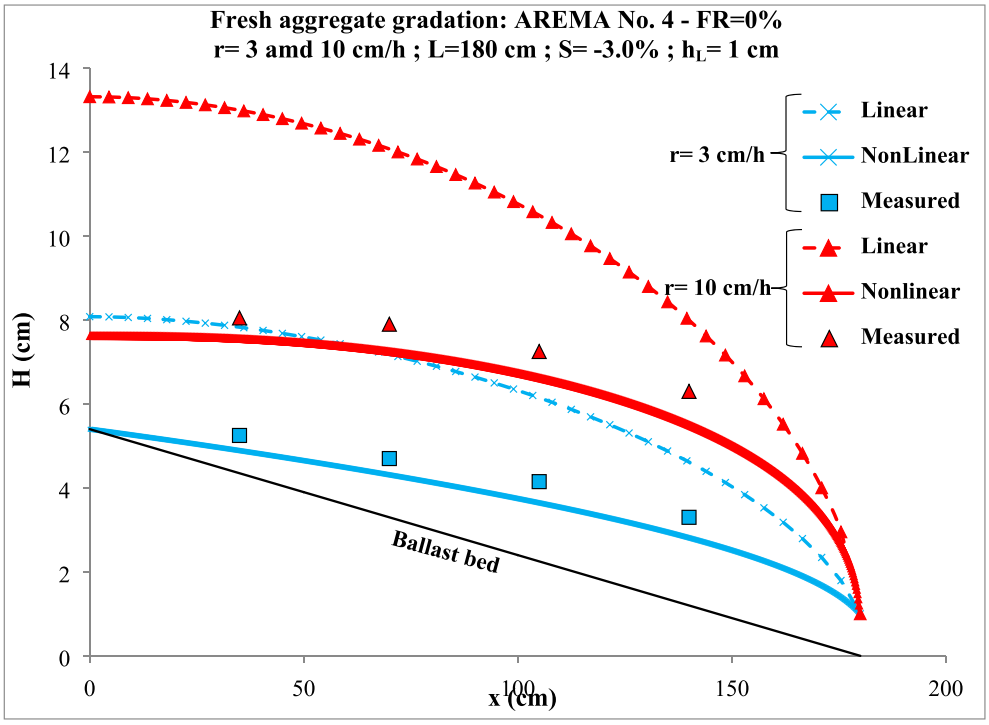

a AREMA No. 4

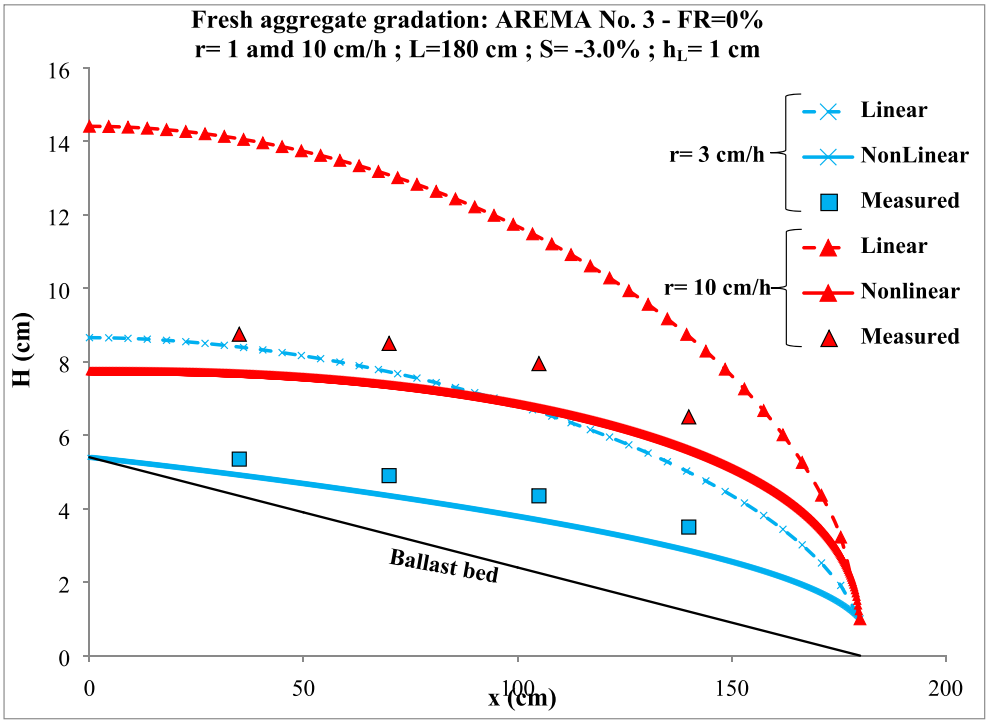

b AREMA No. 3

Fig. 10. Water level along the cross-section of the ballast layer comprising clean ballast particles.

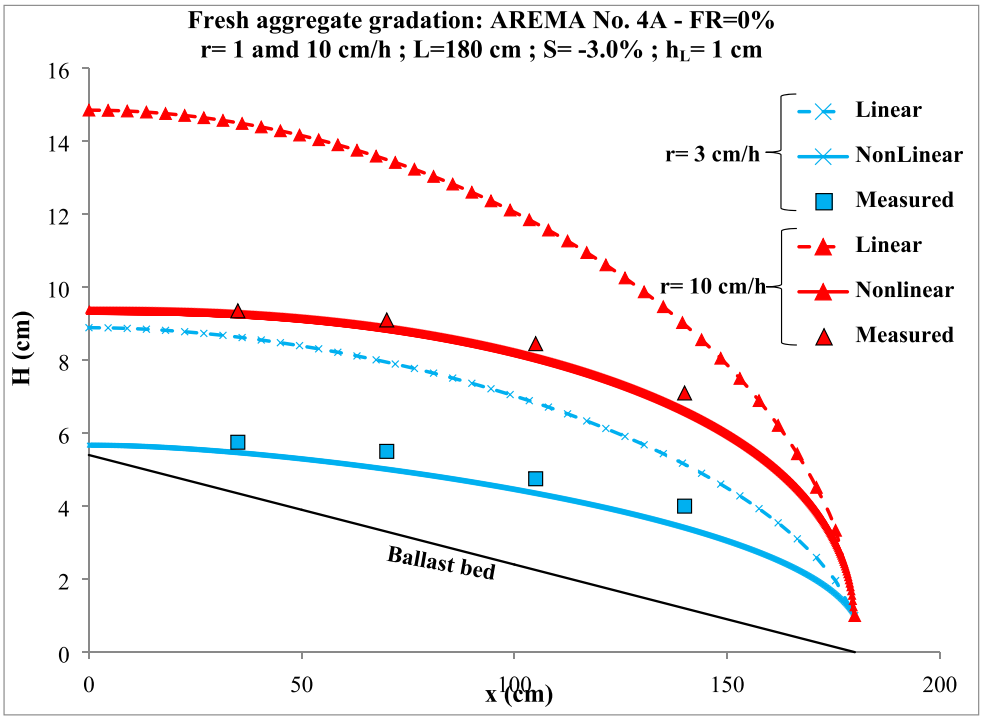

c AREMA No. 4A

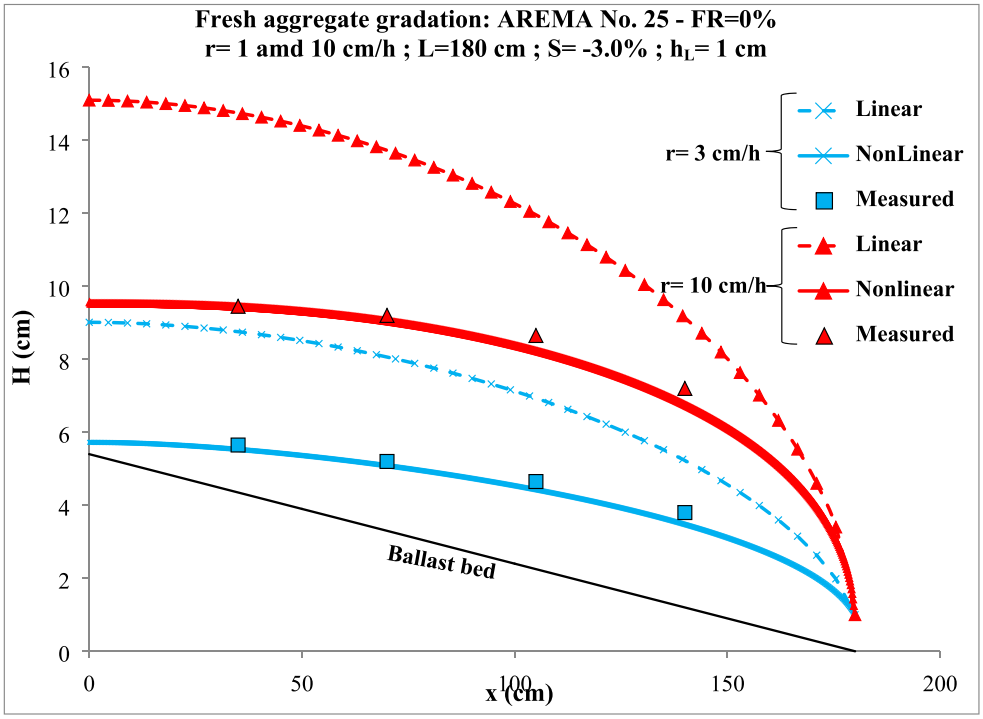

d AREMA No. 25

Fig. 10. (*continued*).

Finally, considering $\eta = 2$, representing the turbulent flow condition, the Eq. (8) is presented as follows:

$$\frac{dx}{x} = \frac{\eta^2.d\eta}{-c_1 r^2 - s\eta^2 - \eta^3} \quad (17)$$

For clean ballast particles, the exponent of the power law (n) was set to 2 and 1.7, depending on the aggregate gradation, to reflect the nonlinear flow regime. Fig. 10 clearly illustrates that using the nonlinear model in the A-N approach aligns more closely with water level measurements from the flume test than the linear model. In this context, Li et al. [28] highlighted the post-Darcian flow phenomenon when large-sized pores form due to an increased contribution from the inertial

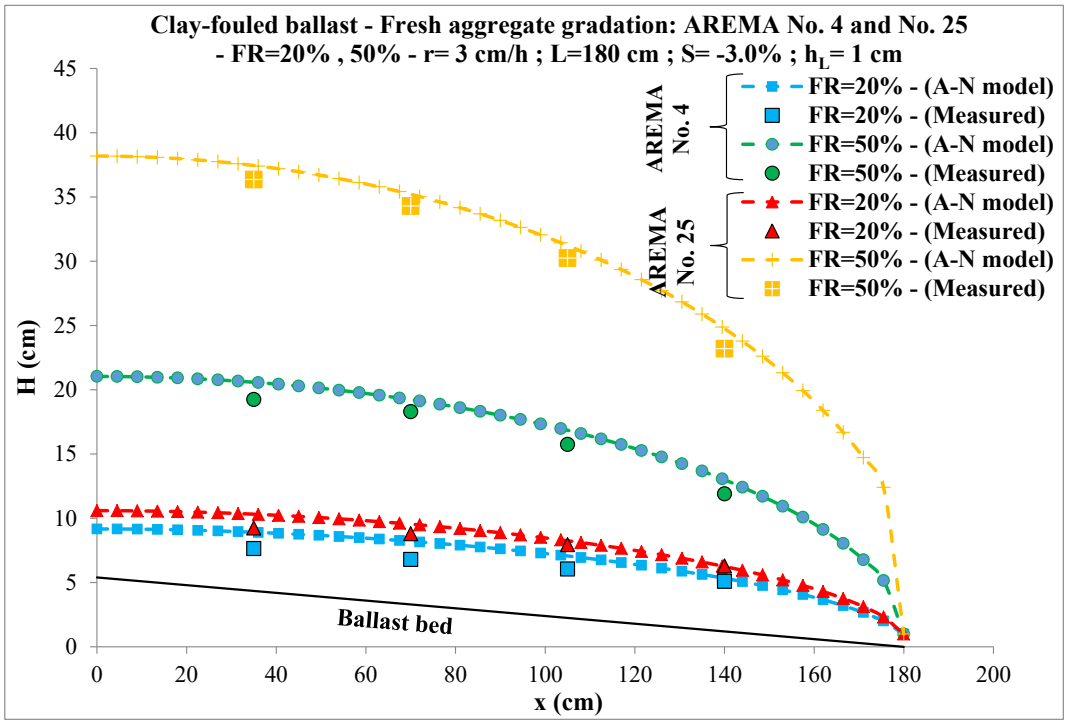

a r= 3 cm/h

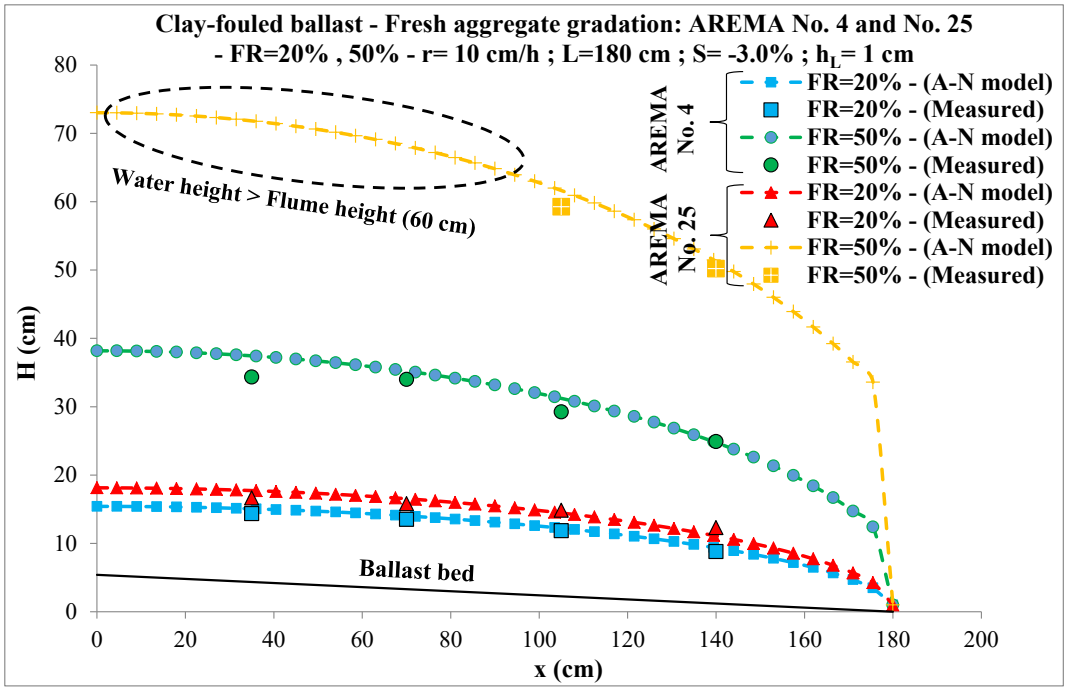

b r= 10 cm/h

Fig. 11. Water level along the cross-section of the ballast layer comprising clay-fouled ballast particles.

force. Consequently, clean ballast does not follow the linear Darcy's law due to the increased momentum transference, resulting in a rise in flow rate that is less than the estimated value from the established linear model. Wang et al. [42] observed the same trend in groundwater flow studies. Moreover, the difference in water height between various gradations of fresh ballast is insignificant, both in experimental measurements and A-N estimations.

For clay-fouled ballast, the integration of a linear model into the A-N approach effectively approximates the water height due to a reduction in the turbulence of water movement, as illustrated in Fig. 11. As expected, an appreciable increase in water level is observed as FR values rise. In this scenario, the initial gradation of ballast emerges as a significant variable. Considering the acceptable limit of permeability of fouled ballast to be as low as 10^{-2} cm/s [1,35], the hydraulic

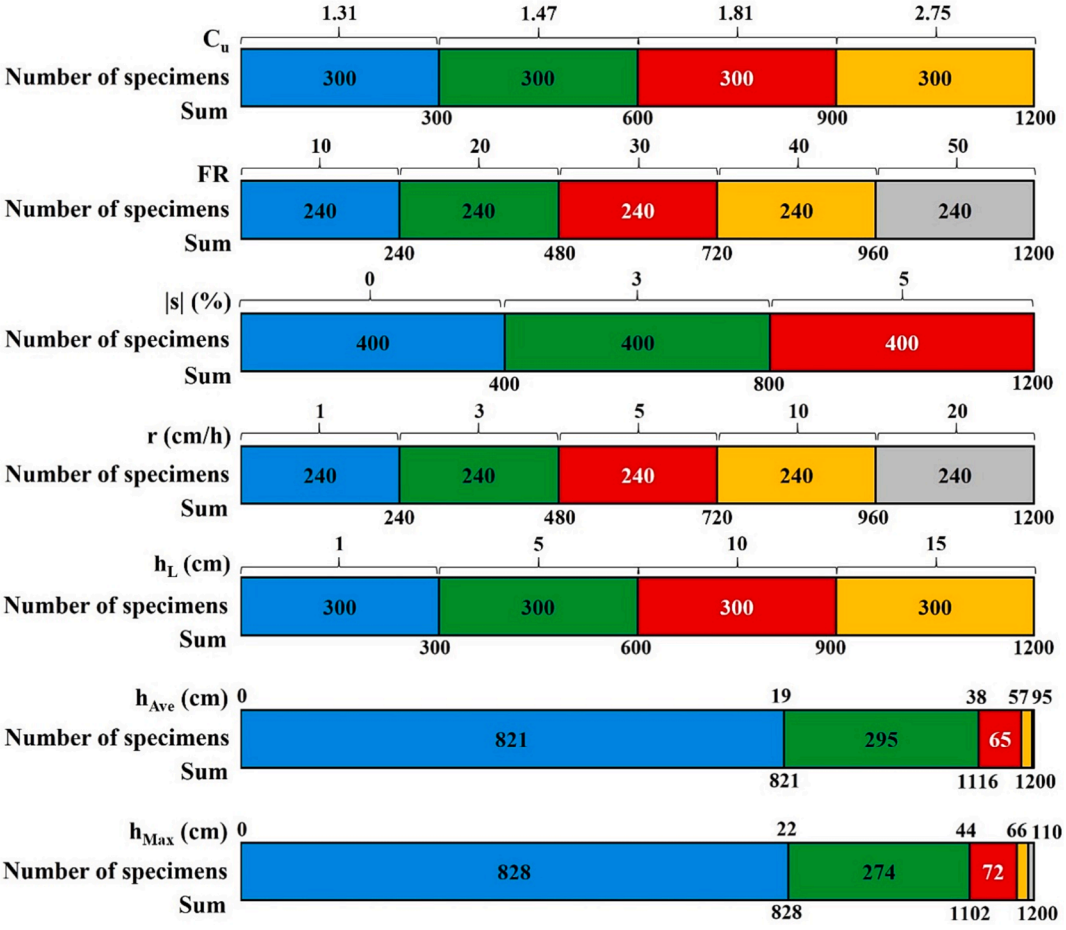

Fig. 12. Range of inputs and outputs for training and testing the ML models.

Table 4
Performance indices of characterized ML models.

ML model	h_{Ave}						h_{Max}					
	R^2		RMSE		VAF		R^2		RMSE		VAF	
	Train	Test	Train	Test	Train	Test	Train	Test	Train	Test	Train	Test
RFR	0.999	0.989	0.434	1.325	99.94	99.28	0.999	0.992	0.486	1.322	99.95	99.54
SVR	0.972	0.959	2.382	2.488	96.85	96.65	0.963	0.962	2.939	2.934	96.93	97.05
XGBoost	0.999	0.998	0.325	0.479	99.97	99.93	0.999	0.998	0.381	0.612	99.97	99.92

conductivity values of all clay-fouled ballast specimens (as presented in Table 3.b) are within the acceptable range, but the water height rises above the ballast surface under moderately to highly fouled conditions. As highlighted by Tennakoon et al. [37], the critical condition for maintenance implementation occurs when the VCI exceeds 50 %. Given the physical properties of the ballast and kaolin materials used in this study, this contamination level is reached when the FR value is greater than 30 %. Under heavy rainfall rates, such as 10 cm/h, nearly half of the ballast thickness is saturated even when the FR is only 20 %. As noted by Li et al. [26], the increased settlement of fouled ballast is due to the presence of water in this granular layer.

Generation of dataset

The validated A-N approach was utilized to generate the characterized outputs, including the average water height (h_{Ave}) and the maximum water height (h_{Max}). Fig. 12 displays the statistical distributions of the considered input variables and the computed outputs based on the A-N approach, assuming a laminar flow regime. Indeed, previous discussions on the results of hydraulic conductivity and water height from permeability and flume tests have demonstrated that Darcy's law can effectively account for water flow through clay-fouled ballast.

Results of ML models

Training and testing the ML models

The ML models were implemented using the Python programming language to develop the optimal structures. The grid search method was employed to determine the most suitable parameters for each specific ML model. For the RFR, optimal values were characterized as a n_estimators of 50, a max_depth of 10, and a min_samples_leaf of 1. For SVR, the optimal values of C and gamma were determined to be 10 and 0.1, respectively. The XGBoost structure was developed by tuning the hyperparameters, resulting in 100 trees, a maximum depth of 4, and a learning rate of 0.1.

Table 4 summarizes the performance indices computed based on the differences between estimations of the A-N approach and predictions of the ML models, validating XGBoost as the most suitable model. Fig. 13 shows the calculated as well as the predicted values of water height

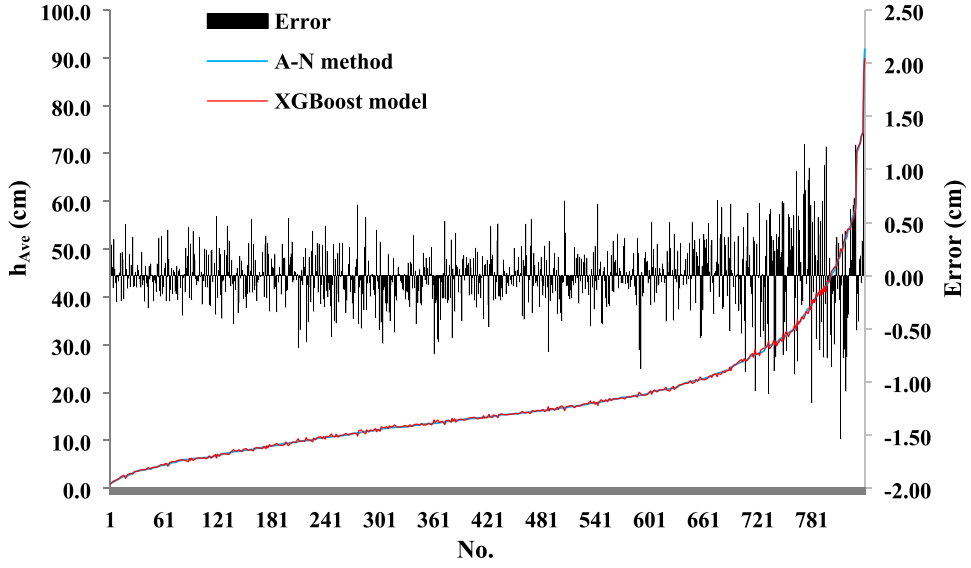

a h_{Ave}

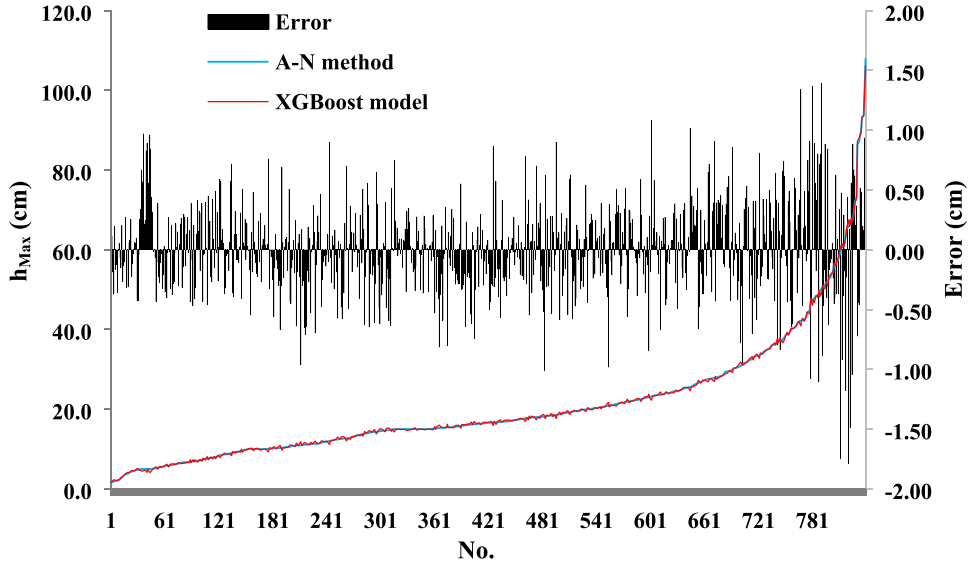

b h_{Max}

Fig. 13. Variation of the differences between computed (based on the A-N solution) and predicted (based on the XGBoost model) values of water level in an ascending form - training data set.

based on XGBoost for the training dataset, with all estimations arranged in ascending order. Similarly, Fig. 14 illustrates the estimated water levels versus the predicted ones for the testing dataset, confirming an error of less than 10 %.

Discussion on factor of importance for characterized variables

The influence of specific inputs, including ballast gradation, fouling ratio, ballast bed slope, rainfall rate, and boundary condition are assessed using the best-performing ML model, i.e., XGBoost. As illustrated in Fig. 15, the most influential parameter for h_{Ave} is the rainfall rate, followed by the fouling ratio. However, this order varies in the case of h_{Max}, where FR has a higher influence. On the contrary, the ballast bed slope is the least influential variable compared to all other factors for the water level prediction using the XGBoost model. As pointed out by Gong et al. [12], the simulation of water movement through a typical track section by establishment of computational fluid dynamics (CFD) confirmed the critical effect of fouling index on lateral flow rate. Fig. 16 provides more detailed insights into the influence of individual variables based on the SHAP values. Notably, fouling ratio and rainfall rate are crucial variables; increases in these values lead to higher water levels. Also, an increase in C_u, indicative of a wider range of particle sizes, results in a rise in water height, though this effect is relatively minor. As noted by Shi et al. [36], a C_u value of 2.2 optimizes drainage capacity while minimizing ballast breakage, as long as a suitable drainage system is provided along the track and highly fouled conditions are prevented. The SHAP values of C_u and h_L indicate an exacerbated boundary effect in

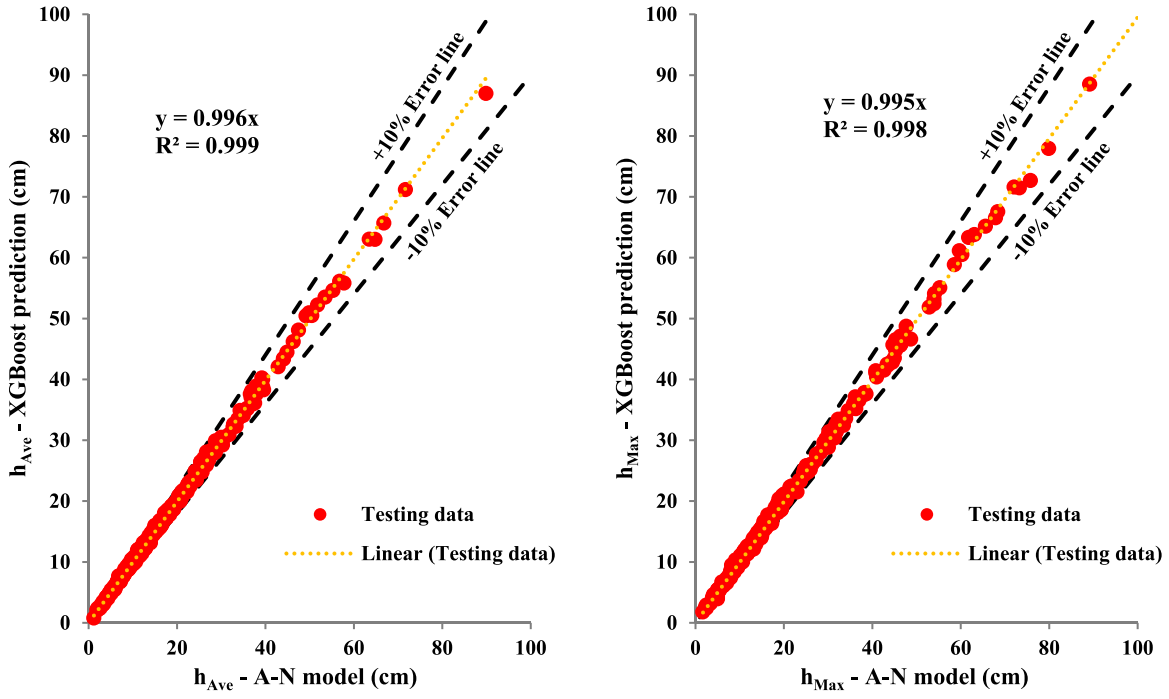

a h_{Ave} b h_{Max}

Fig. 14. Observed versus predicted water height by establishment of A-N approach and the elite ML model (XGBoost) - Testing dataset.

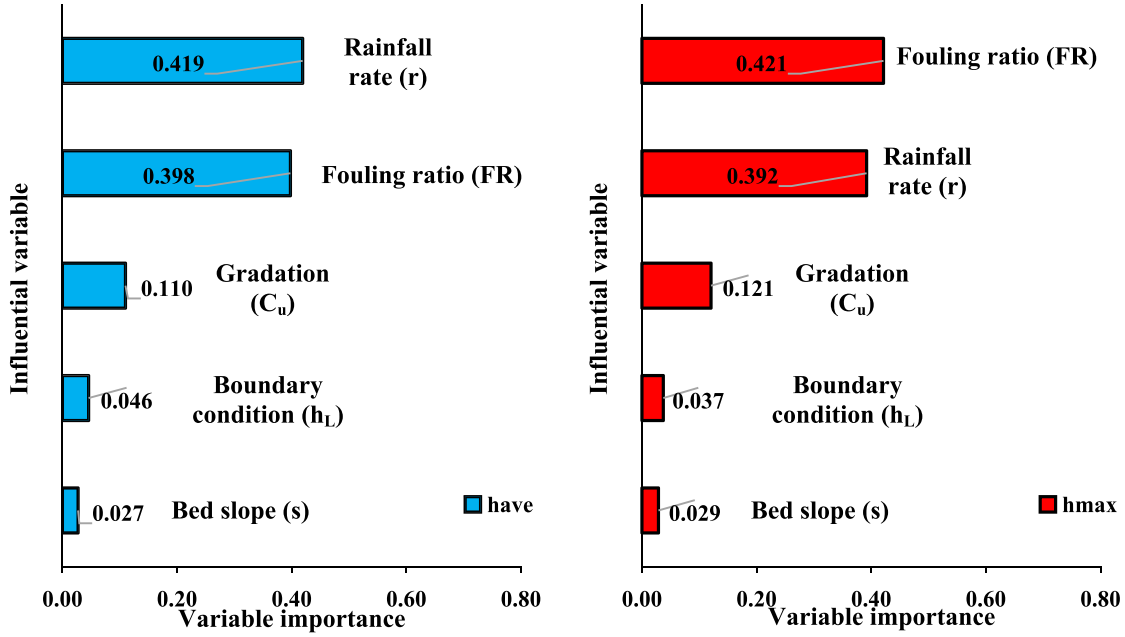

a h_{Ave} b h_{Max}

Fig. 15. Factor of importance derived based on the elite ML model (XGBoost).

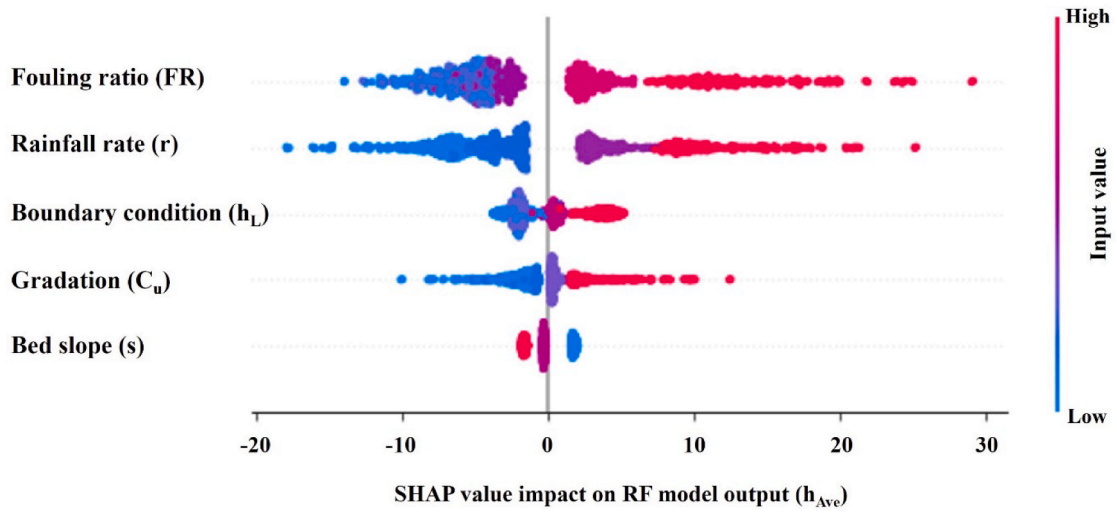

a Average water height (h_{Ave})

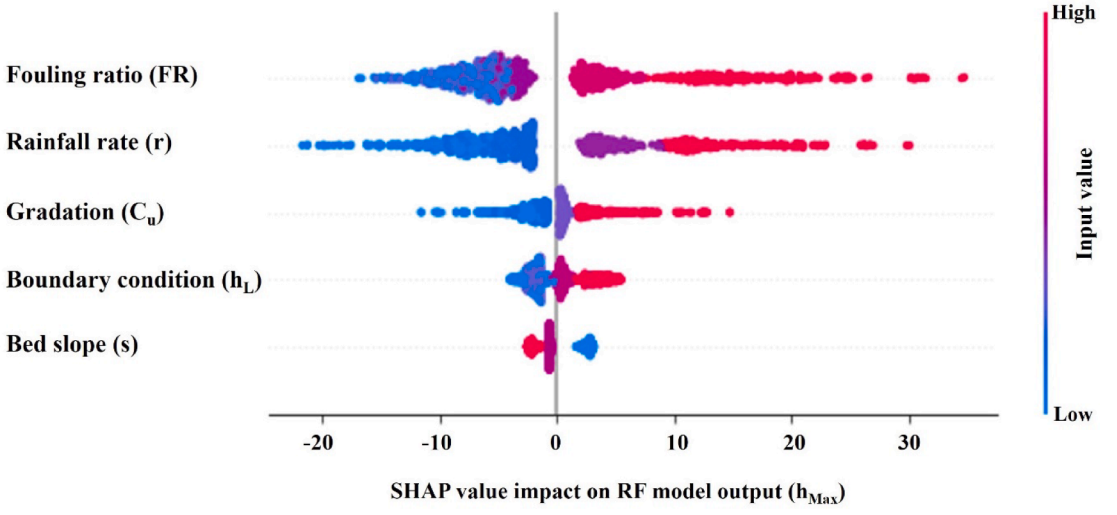

b Maximum water height (h_{Max})

Fig. 16. Summary plot of SHAP values of characterized inputs for each specific row of dataset based on the XGBoost model - Red colour representing the higher values of input, blue colour representing lower values of input. (For interpretation of the references to colour in this figure legend, the reader is referred to the web version of this article.)

the case of h_{Ave}, as water ponding on the side ditch results in a more uniform water level throughout the ballast layer cross-section. Furthermore, the slope of the ballast bed is inversely proportional to the water height; however, this effect is negligible.

Conclusions

In this study, we investigated the water level in the clay-fouled ballast layer under steady-state conditions using both flume test measurements and calculated values from the validated A-N approach. Various variables were considered, including ballast gradation, fouling ratio, ballast bed slope, rainfall rate, and boundary condition. Machine learning (ML) models, including RFR, SVR, and XGBoost, were used for automatic data processing. In addition, the most effective ML model for ballast drainage capacity estimation was identified. The main conclusions are as follows:

- Clean ballast samples follow a non-laminar flow regime. For accurate water level estimation, it is necessary to use Izbash's law, which aligns closely with flume test measurements.
- Comparisons between water heights measured via the flume test and those estimated with the A-N approach show that increasing clay fouling enhances the applicability of the conventional linear model, Darcy's law. This trend aligns with the relationship between flow velocity and applied hydraulic head, as established by the constant-head permeability test.
- For a fouling ratio (FR) of 20 %, ballast saturation is significant during heavy rainfall, despite negligible water height recorded at lower rainfall rates. However, an FR of 50 % leads to rising water heights above the ballast surface.
- Aggregate gradation's effect on water height is minor for clean ballast particles, but both flume test measurements and A-N approach estimations confirm its substantial influence under highly-fouled conditions.

- According to predictions from the most effective ML model, XGBoost, fouling ratio and rainfall rate are the key factors affecting water height in clay-fouled ballast.
- More uniform gradation and a steeper ballast bed slope predict lower water height values, but their effects are less significant than the influence of the fouling ratio and rainfall rate.

CRediT authorship contribution statement

Mehdi Koohmishi: Writing – original draft, Visualization, Software, Methodology, Investigation, Data curation. **Yunlong Guo:** Writing – review & editing, Visualization, Supervision, Project administration, Methodology, Funding acquisition, Conceptualization.

Declaration of Competing Interest

The authors declare that they have no known competing financial interests or personal relationships that could have appeared to influence the work reported in this paper.

Data availability

Data will be made available on request.

Acknowledgements

The European Commission and UKRI Engineering and Physical Science Research Council (EPSRC) are acknowledged for the financial sponsorship of Re4Rail project (Grant No EP/Y015401/1).

References

[1] Anbazhagan P, Indraratna B, Rujikiatkamjorn C, Su L. Using a seismic survey to measure the shear modulus of clean and fouled ballast. Geomech. Geoeng.: Int. J. 2010;5(2):117–26.
[2] Araya SN, Ghezzehei TA. Using machine learning for prediction of saturated hydraulic conductivity and its sensitivity to soil structural perturbations. Water Resour Res 2019;55(7):5715–37.
[3] AREMA. (2010). *Manual for railway engineering, Vol. 1: Track, Ch. 1: Roadway and Ballast*: American Railroad Engineering and Maintenance of Way Association (AREMA), Washington, D.C.
[4] Javad Azarhoosh M, Koohmishi M. Prediction of hydraulic conductivity of porous granular media by establishment of random forest algorithm. Constr Build Mater 2023;366:130065.
[5] Breiman L. Random forests. *Machine learning* 2001;45:5–32.
[6] Charbeneau RJ, Barrett ME. Drainage hydraulics of permeable friction courses. Water Resour Res 2008;44(4).
[7] Chen T, Guestrin C. Xgboost: A scalable tree boosting system. Paper presented at the Proceedings of the 22nd acm sigkdd international conference on knowledge discovery and data mining. 2016.
[8] Danesh A, Palassi M, Mirghasemi AA. Effect of sand and clay fouling on the shear strength of railway ballast for different ballast gradations. Granul Matter 2018;20:1–14.
[9] Danquah, W., Ghataora, G., and Burrow, M. (2014). *The effect of ballast fouling on the hydraulic conductivity of the rail track substructure.* Paper presented at the Proceedings of the XV Danube-European Conference on Geotechnical Engineering (DECGE), Austrian Society for Soil Mechanics and Geotechnical Engineering, Vienna, Austria.
[10] Darcy H. Les Fontaines Publiques de la Ville de Dijon. In. Paris: Dalmont; 1856.
[11] Fwa T, Tan S, Chuai C. Permeability measurement of base materials using falling-head test apparatus. Transp Res Rec 1998;1615(1):94–9.
[12] Gong Y, Qian Yu, Fanucci F. Investigation on the drainage condition within the ballast layer based on 3D CFD simulations. Transp Geotech 2023;39:100939.
[13] Heyns FJ. Railway track drainage design techniques. University of Massachusetts Amherst; 2000.
[14] Hu, Y., Li, K., Zhang, B., and Han, B. (2022). Investigation of the strength of concrete-like material with waste rock and aeolian sand as aggregate by machine learning. *Journal of Computational Design and Engineering, 9*(5), 2134-2150.
[15] Huang H, Moaveni M, Schmidt S, Tutumluer E, Hart JM. Evaluation of Railway Ballast Permeability Using Machine Vision-Based Degradation Analysis. Transp Res Rec 2018;2672(10):62–73.
[16] Huang H, Tutumluer E. Discrete element modeling for fouled railroad ballast. Constr Build Mater 2011;25(8):3306–12.
[17] Huang H, Tutumluer E, Dombrow W. Laboratory characterization of fouled railroad ballast behavior. Transp Res Rec 2009;2117(1):93–101.
[18] Indraratna B, Rujikiatkamjorn C, Salim W. Advanced rail geotechnology–ballasted track. CRC Press; 2023.
[19] Indraratna B, Singh M, Nguyen TT. The mechanism and effects of subgrade fluidisation under ballasted railway tracks. Railway Engineering Science 2020;28(2):113–28.
[20] Indraratna B, Tennakoon N, Nimbalkar S, Rujikiatkamjorn C. Behaviour of clay-fouled ballast under drained triaxial testing. Géotechnique 2013;63(5):410–9.
[21] Izbash, S. (1931). O Filtracii Kropnozernstom Materiale. In. Leningrad, USSR.
[22] Jiang Xi, Zhu H, Yan Z, Zhang F, Ye F, Li P, et al. A state-of-art review on development and progress of backfill grouting materials for shield tunneling. Developments in the Built Environment 2023;16:100250.
[23] Kardani N, Aminpour M, Nouman Amjad Raja M, Kumar G, Bardhan A, Nazem M. Prediction of the resilient modulus of compacted subgrade soils using ensemble machine learning methods. Transp Geotech 2022;36:100827.
[24] Koohmishi M. Drainage potential of degraded railway ballast considering initial gradation and intrusion of external fine materials. Soils Found 2019;59(6):2265–78.
[25] Koohmishi M, Palassi M. Effect of gradation of aggregate and size of fouling materials on hydraulic conductivity of sand-fouled railway ballast. Constr Build Mater 2018;167:514–23.
[26] Li D, Hyslip J, Sussmann T, Chrismer S. Railway geotechnics. CRC Press; 2015.
[27] Li Y, Rahardjo H, Satyanaga A, Rangarajan S, Lee D-T. Soil database development with the application of machine learning methods in soil properties prediction. Eng Geol 2022;306:106769.
[28] Li Z, Wan J, Zhan H, Cheng X, Chang W, Huang K. Particle size distribution on Forchheimer flow and transition of flow regimes in porous media. J Hydrol 2019;574:1–11.
[29] Mayuranga HGS, Navaratnarajah SK. Effect of clay fouling on track drainage capacity of railway Ballast: Experimental and numerical study. Constr Build Mater 2023;364:129987.
[30] Menke HP, Maes J, Geiger S. Upscaling the porosity–permeability relationship of a microporous carbonate for Darcy-scale flow with machine learning. Sci Rep 2021;11(1):2625.
[31] Nguyen QH, Ly H-B, Ho LS, Al-Ansari N, Le HV, Tran VQ, et al. Influence of data splitting on performance of machine learning models in prediction of shear strength of soil. Math Probl Eng 2021;2021:1–15.
[32] Parsons RL, Rahman A, Han J, Glavinich TE. Track ballast fouling and permeability characterization by using resistivity. Transp Res Rec 2014;2448(1):133–41.
[33] Qian Y, Mishra D, Tutumluer E, Kazmee HA. Characterization of geogrid reinforced ballast behavior at different levels of degradation through triaxial shear strength test and discrete element modeling. Geotext Geomembr 2015;43(5):393–402.
[34] Rahman, A., Parsons, R., and Han, J. (2012). *Properties of fouled railroad ballast (phase 1)*. Retrieved from.
[35] Selig ET, Waters JM. Track geotechnology and substructure management. Thomas Telford; 1994.
[36] Shi C, Fan Z, Connolly DP, Jing G, Markine V, Guo Y. Railway ballast performance: recent advances in the understanding of geometry, distribution and degradation. Transp Geotech 2023;41:101042.
[37] Tennakoon N, Indraratna B, Rujikiatkamjorn C, Nimbalkar S, Neville T. The Role of Ballast-Fouling Characteristics on the Drainage Capacity of Rail Substructure. Geotech Test J 2012;35(4):104107.
[38] Tian J, Qi C, Sun Y, Yaseen ZM, Pham BT. Permeability prediction of porous media using a combination of computational fluid dynamics and hybrid machine learning methods. Eng Comput 2021;37(4):3455–71.
[39] Vakharia V, Gujar R. Prediction of compressive strength and portland cement composition using cross-validation and feature ranking techniques. Constr Build Mater 2019;225:292–301.
[40] Vapnik VN, editor. The Nature of Statistical Learning Theory. New York, NY: Springer New York; 2000.
[41] Venuja S, Navaratnarajah SK, Bandara CS, Jayasinghe JASC. Experimental and numerical study on the shear-strain behavior of ballast with different gradations. In: International Conference on Sustainable Built Environment. Springer Nature Singapore: Singapore; 2022. p. 245–54.
[42] Wang X, Qian J, Ma H, Ma L, Zhou D, Sun HongGuang. Prediction of post-Darcy flow based on the spatial non-local distribution of hydraulic gradient: Preliminary assessment of wastewater management. Chemosphere 2023;334:139013.
[43] Yang J, Ishikawa T, Tokoro T, Nakamura T, Kijiya I, Okayasu T. Effect evaluation of drainage condition and water content on cyclic plastic deformation of aged ballast and its estimation models. Transp Geotech 2021;30:100606.
[44] Zhao W, Qiang W, Yang F, Jing G, Guo Y. Data-driven ballast layer degradation identification and maintenance decision based on track geometry irregularities. International Journal of Rail Transportation 2023:1–23.